Chapter 4

Results and discussion

4.1 Characterization of Pb-based ferroelectric powders

4.1.1 Particle size and particle size distribution

There were 3 types of Pb-based ferroelectric powders used in this study. They were ACL 4040, ACL 4050, and ACL 4055. The milling process has been done in a ball mill for 18 and 72 hours. The powders were then dried in an electric oven, and after drying they were ground in a mortar one more time. These powders were characterized for particle size and particle size distribution (PSD) by the mastersizer (MALVERN Instruments: Mastersizer-S). The results are shown in Table 4.1.

Table 4.1 Particle size and particle size distribution of Pb-based ferroelectric powders before and after milling

Type of powders	Milling time (hours)	Average particle size, D[4,3] (μm)	Range of particle size (μm)
ACL 4040	None	3.74	0.23-14.22
	18	1.23	0.31-3.60
	72	0.28	0.05-0.78
ACL 4050	None	5.34	0.78-56.23
	18	1.13	0.27-3.09
ACL 4055	None	4.88	0.78-14.22
	18	1.46	0.27-4.19
	72	0.39	0.05-1.95

From Table 4.1, the particle sizes of all powders were reduced after milling and they were even smaller when milling time increased. Moreover, the particle size distribution after milling was found to be narrower than before milling.

4.1.2 X-ray diffraction and SEM study

As-received powders were examined for phases and crystal structures by x-ray diffractometer (CuK_α ; JEOL: JDX-3530). The x-ray diffraction patterns of all powders are shown in Fig. 4.1.

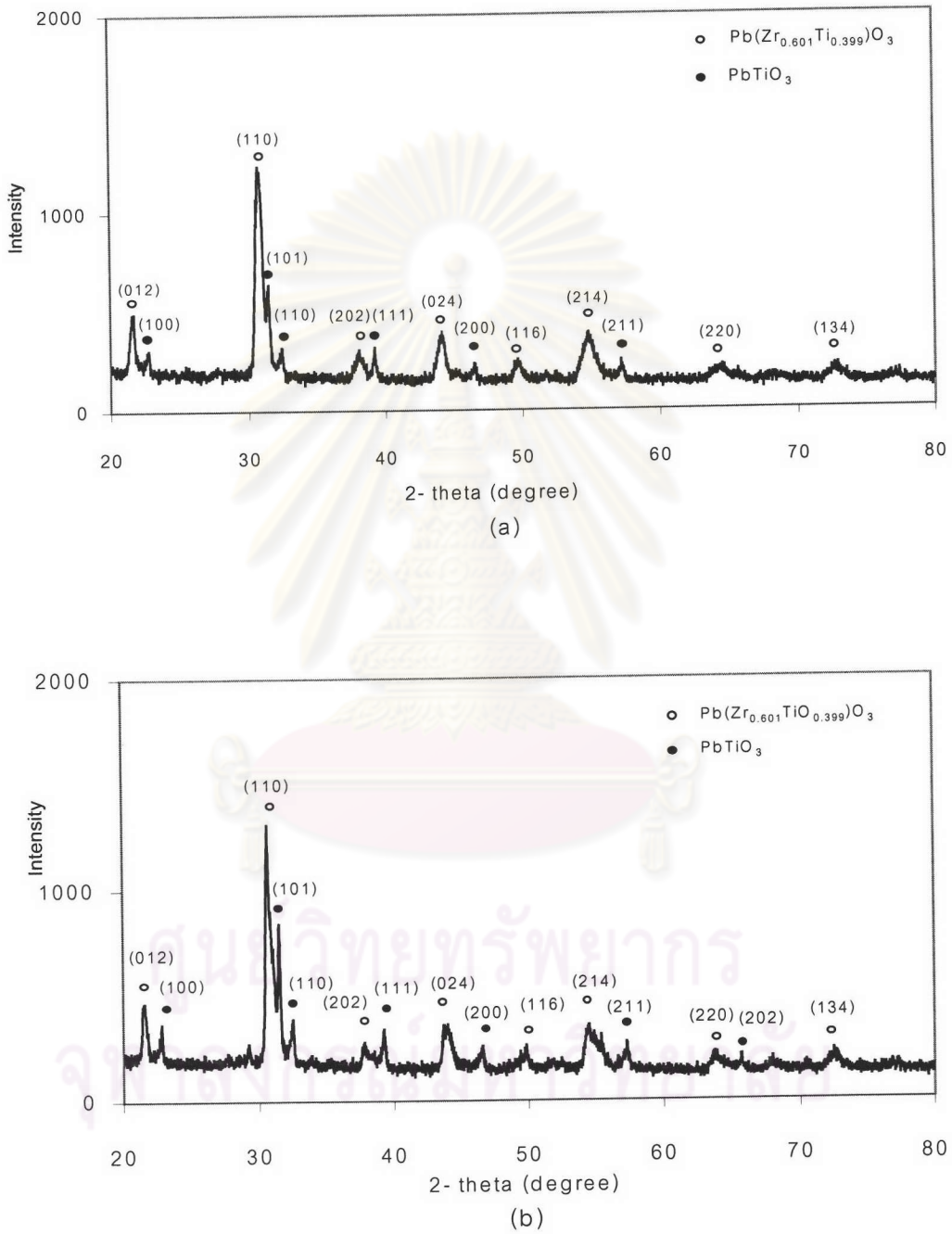

Fig. 4.1 XRD patterns of (a) ACL 4040 powder and (b) ACL 4050 powder

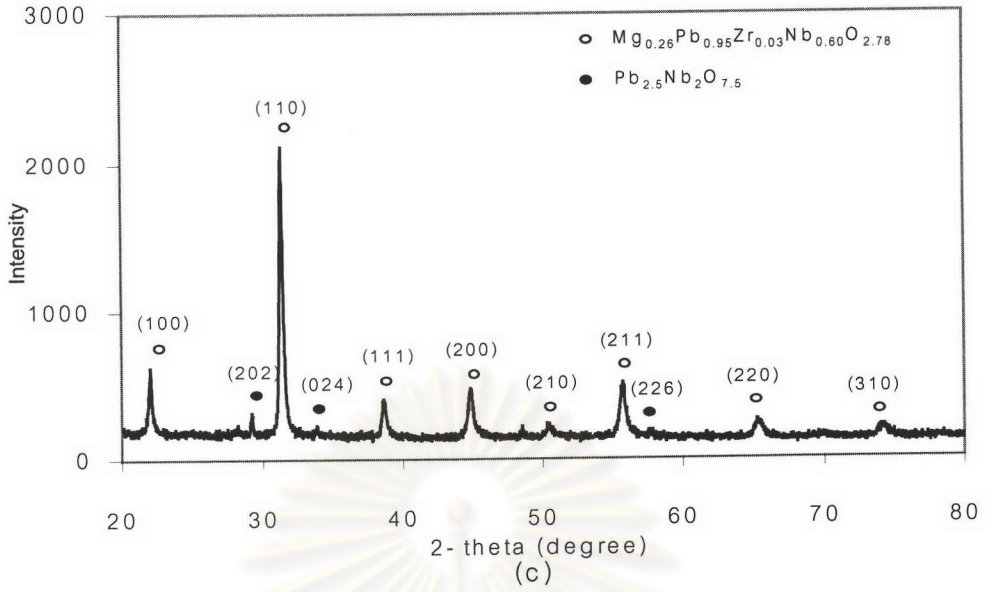

Fig. 4.1 XRD patterns of (c) ACL 4055 powder

The XRD patterns of ACL 4040 powder and ACL 4050 powder show a mixture of Pb $(Zr_{0.601}Ti_{0.399})O_3$;PZT (PDF No.89-1280) and $PbTiO_3$ (PDF No.75-0438). For ACL 4055 powder, the pattern shows a composition of $Mg_{0.26}Pb_{0.95}Zr_{0.03}Nb_{0.60}O_{2.78}$ (PDF No.48-0132) and $Pb_{2.5}Nb_2O_{7.5}$ (PDF No.40-0831). Also, SEM micrographs of them are shown in Fig. 4.2.

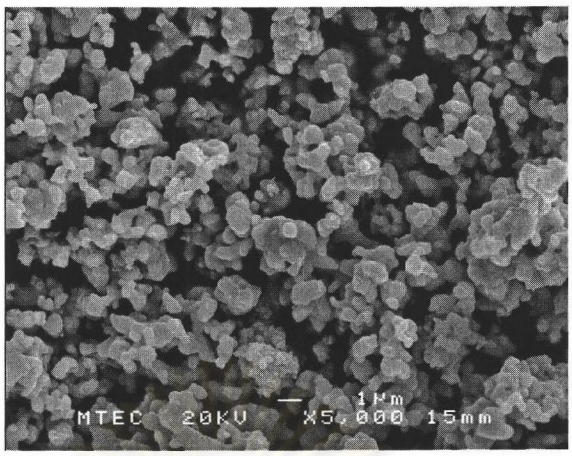

(a)

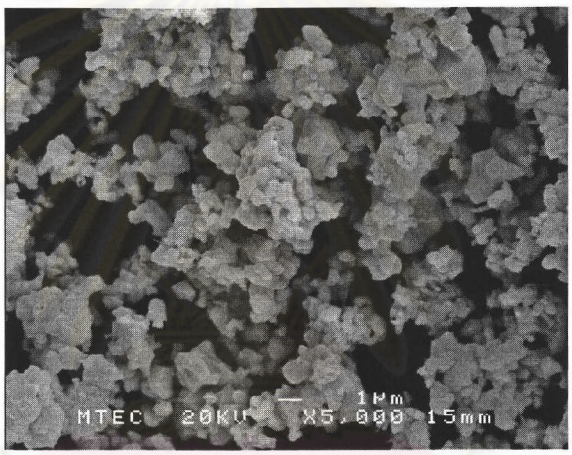

(b)

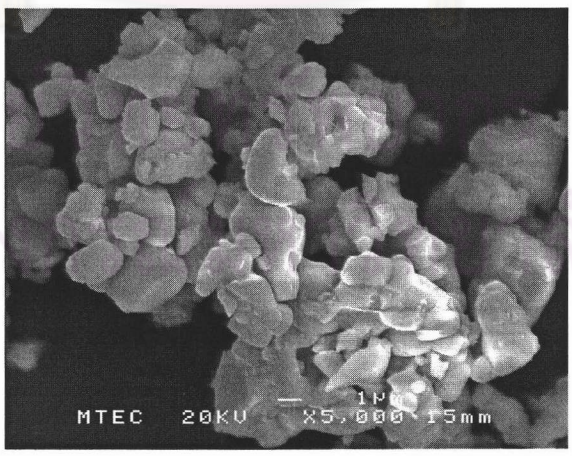

(c)

Fig. 4.2 SEM micrographs of (a) ACL 4040, (b) ACL 4050, and (c) ACL 4055 powders

4.2 Characterization of stainless steel substrates

The stainless steel substrates before and after firing at 680°C, 750°C, 800°C, and 850°C for 1 hour were also characterized by the x-ray diffractometer. The x-ray diffraction patterns are illustrated in Fig. 4.3. This figure shows Fe-Cr (PDF No.34-0396) and Fe,syn (PDF No.06-0696) for all samples. The second phase, however, occurred after firing at 850°C. Its x-ray diffraction pattern corresponded to Fe_2O_3 (PDF No.33-0664) phase. This phase might come from the reaction between Fe and O_2 in air during firing at high temperature. Therefore, it should be awared that if using the stainless steel as substrate, the firing temperature should not exceed 800°C to prevent the chemical reaction at the surface of the substrate and air.

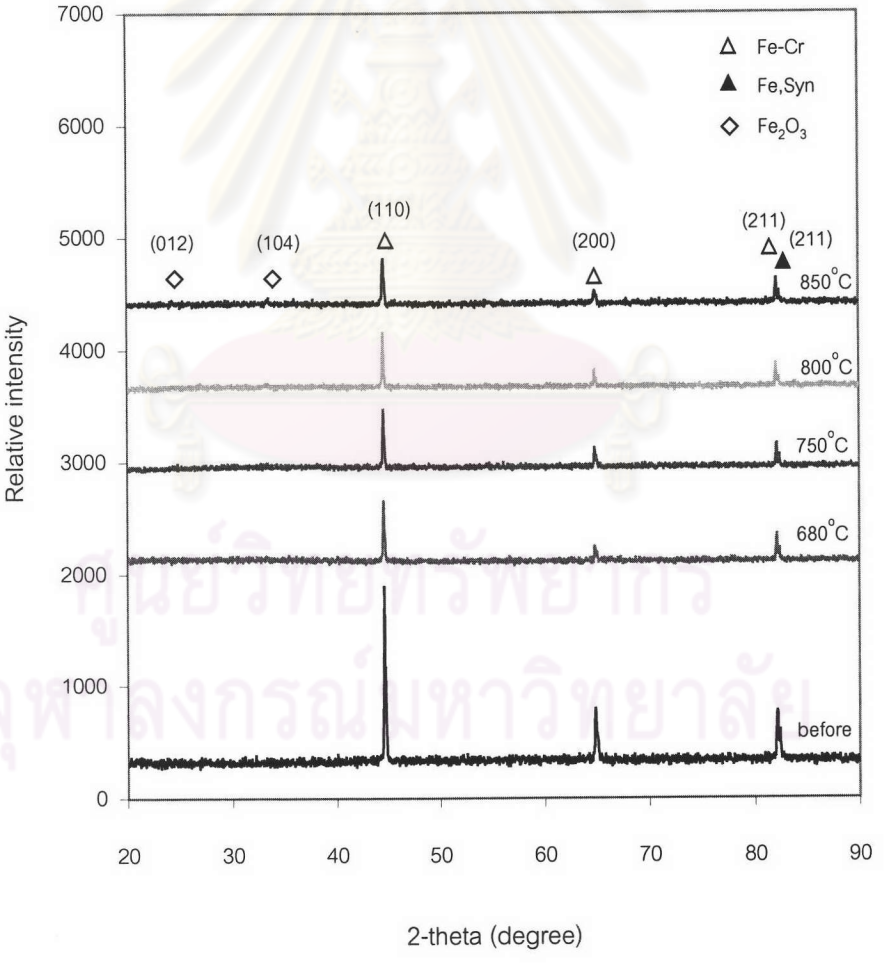

Fig. 4.3 XRD patterns of stainless steel substrates before and after firing at 680°C, 750°C, 800°C, and 850°C for 1 hour

4.3 Characterization of Pb-based ferroelectric thick films

There were many paste formulas prepared in this study. The main paste formulas are given in Table 4.2. The pastes were screen-printed onto stainless steel substrates, and then dried at 100°C for 2 hours in order to remove the solvent. Pb-based ferroelectric thick films on stainless steel substrates were fired at different temperatures to remove the organic binder and increase densification. The Pb-based ferroelectric pastes and thick films were characterized in the next step.

Table 4.2 Main Pb-based ferroelectric paste formulas in this study

Paste formulas	Compositions				
	Pb-based ferroelectric powders	Frit (wt%)	TE2* (wt%)	TE4** (wt%)	Phosphate ester (wt%)
APA	As-received ACL 4040	-	17.04	-	-
APB	18 hour milled ACL 4040	-	17.04	-	-
APC	72 hour milled ACL 4040	-	17.04	-	-
KPA	As-received ACL 4050	-	18.86	-	-
KPB	18 hour milled ACL 4050	-	18.86	-	-
UPA	As-received ACL 4055	-	15.03	-	-
UPB	18 hour milled ACL 4055	-	15.02	-	-
UPC	72 hour milled ACL 4055	-	20.01	-	-
UPB8	18 hour milled ACL 4055	-	-	12.01	-
UPB8E	18 hour milled ACL 4055	-	-	9.53	0.52
UPB8F	18 hour milled ACL 4055	3.00	-	12.01	-
UPB8EF1	18 hour milled ACL 4055	3.56	-	10.49	0.56

* TE2 is composed of 90 wt% terpineol and 10 wt% ethyl cellulose

** TE4 is composed of 95 wt% terpineol and 5 wt% ethyl cellulose

4.3.1 Effect of Pb-based ferroelectric particle size and particle size distribution on paste compositions

The Pb-based ferroelectric powders (ACL 4040, ACL 4050, and ACL 4055) were separated into 3 parts. They were as-received powders (average particle size about 4-5 μm), 18 hour milled powders (average particle size about 1.0-1.5 μm), and 72 hour milled powders (average particle size about 0.3-0.4 μm). These powders were mixed with organic vehicles and screen-printed onto stainless steel substrates. The optimum paste formulas were observed that they were not too viscous and were easily screen-printed onto the substrates. The high solid loading is the most desirable in order to give good dielectric constants; however, we have to be awared that high solid loading also increases the paste viscosity.

In this screen printing procedure, a squeegee traveled over the screen, the pastes were pushed through the screen and were deposited onto the substrate surface. If the viscosity of the pastes was too high, there might be some paste stuck the screen mesh during its snap-off from the substrates and a defect occurred as shown in Fig. 4.4. This defect was occurred after the screen printing about 4 pieces on the stainless steel substrates in a row under same mask screen (5 x 5 mm^2).

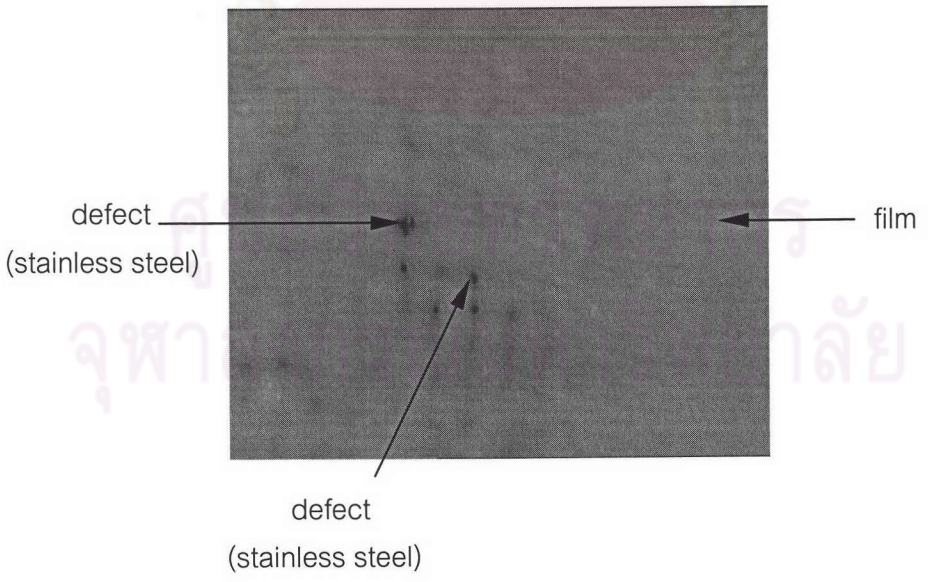

Fig. 4.4 A defect of Pb-based ferroelectric thick films from too high viscosity pastes

The optimum quantity of Pb-based ferroelectric powders in paste compositions was determined physically from thick film surfaces after printing. A good printable paste composition should not give the defect-looks same as in Fig. 4.4 during 15 pieces of stainless steel substrates which were screen-printed in a row under same mask screen. The optimum quantity of ferroelectric powders in the paste is given in Table 4.3. The 18 hour milled powders had the most suitable particle size and particle size distribution for preparing the paste formulas because they gave the highest solid loading in the pastes when compared with as-received powders and 72 hour milled powders including ACL 4040, ACL 4050, and ACL 4055. This phenomenon might due to particle size distribution and particle size of powders. Finer particles must be small enough to enter into all regions of the interstices for increasing particle packing density.[40] However, smaller particles require considerably more vehicle to wet the surface leaving less vehicle for flow and viscosity control.[41]

Table 4.3 Optimum quantity of Pb-based ferroelectric powders in paste compositions

Type of powders	Optimum quantity (wt%)
As-received ACL 4040	81.65 ± 0.05
18 hour milled ACL 4040	**83.97 ± 0.01**
72 hour milled ACL 4040	81.75 ± 0.04
As-received ACL 4050	79.85 ± 0.02
18 hour milled ACL 4050	**81.12 ± 0.03**
As-received ACL 4055	83.73 ± 0.03
18 hour milled ACL 4055	**84.94 ± 0.06**
72 hour milled ACL 4055	80.08 ± 0.03

4.3.2 Effect of Pb-based ferroelectric particle size on electrical properties

There were 8 main paste formulas for using in this study, such as APA, APB, APC, KPA, KPB, UPA, UPB, and UPC of which compositions were already shown in Table 4.2. The capacitance and dissipation factor of the ferroelectric thick films on stainless steel substrates, which were fired at 750°C for 1 hour were measured by the impedance analyzer. KPA and KPB thick films were not able to characterize by this technique since they peeled off the substrates after firing as shown in Fig. 4.5.

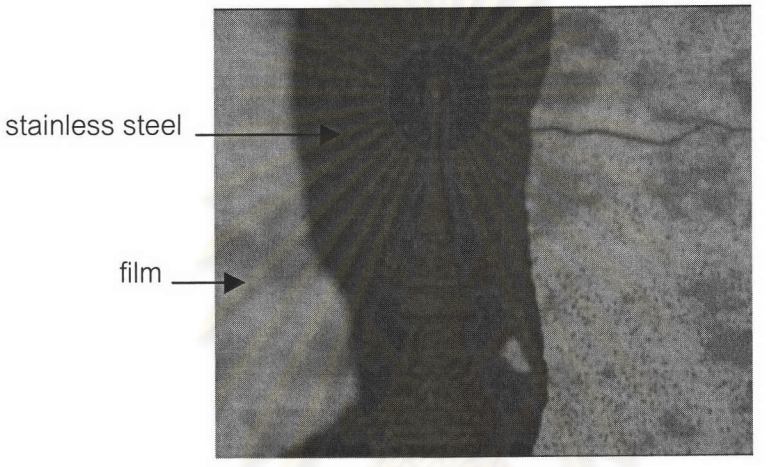

Fig. 4.5 Peeling after fired KPA and KPB thick films 750°C for 1 hour (plane view)

4.3.2.1 ACL 4040 ferroelectric thick films

Fig. 4.6 shows x-ray diffraction patterns of APA, APB, and APC thick films after firing at 750°C for 1 hour. These films showed a mixture of PZT and $PbTiO_3$ similar to ACL 4040 powder; however, second phases were also found. The XRD patterns of these second phases corresponded to Pb_2CrO_5 (PDF No.28-0530) and TiO_2 (PDF No.33-1381).

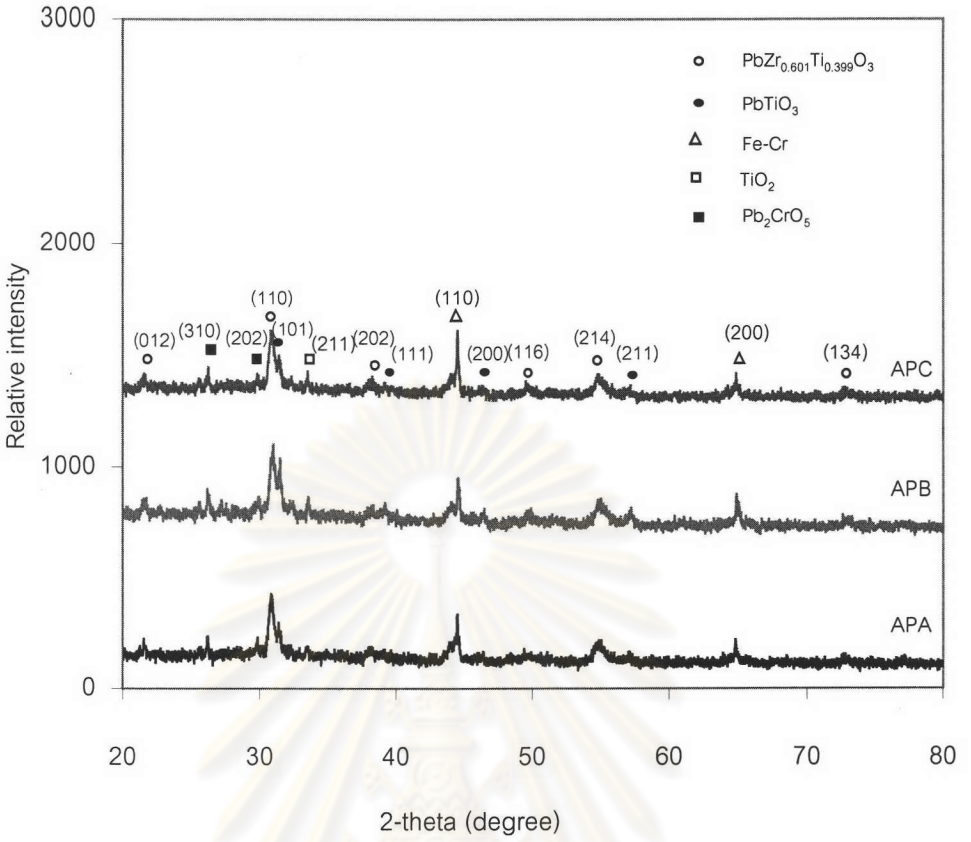

Fig. 4.6 XRD patterns of APA, APB, and APC thick films screen-printed onto stainless steel substrates after firing at 750°C for 1 hour.

Micrographs of the surface of them are illustrated in Fig. 4.7. The grain size of APA was larger than those of APB and APC since the starting powder size was larger. Furthermore, agglomerates were occurred in APA thick film while they were not clearly seen in APB and APC thick films. In addition, all thick films showed abnormally large grains (angular shape) as shown in Fig. 4.7 and were remarkably seen in APB and APC thick films.

The results of energy dispersive spectroscopy (EDS) analysis in Fig.4.8 suggested there were Pb, Cr and O in the abnormally large grains (angular shape), corresponding with XRD patterns, which identified the Pb_2CrO_5 phase. This result confirmed the large grains were Pb_2CrO_5.

The thick films were gold-coated for top electrodes for 120 seconds by sputtering technique, and then the electrical properties were measured by the impedance analyzer at room temperature. These properties were summarized in Fig. 4.9.

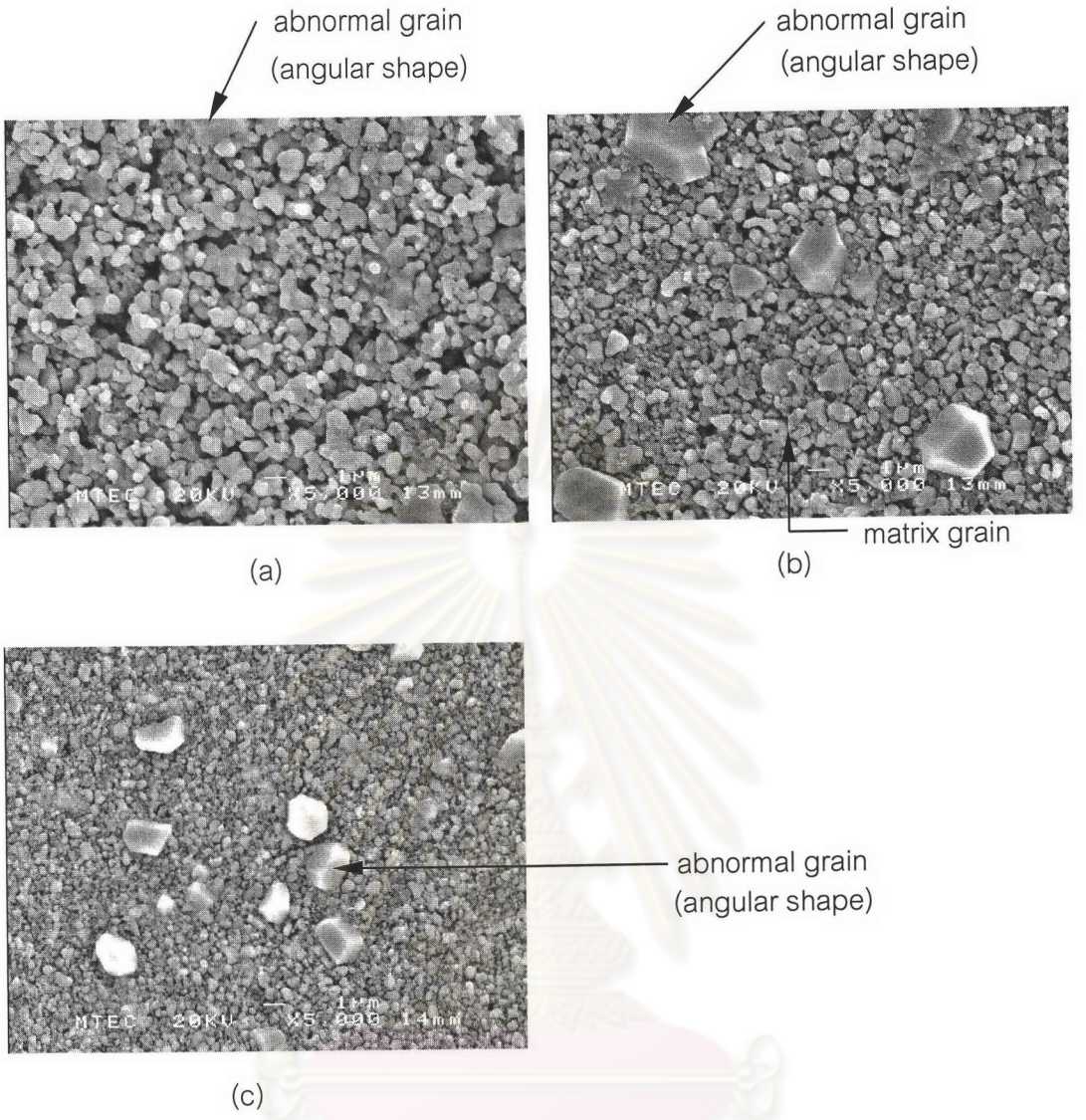

Fig. 4.7 Micrographs of the surface of (a) APA, (b) APB, and (c) APC thick films screen-printed onto stainless steel substrates after firing at 750°C for 1 hour.

Dielectric constants of APA thick films were higher than APB and APC, respectively, while dissipation factors were not significantly different at all frequencies. At 1 kHz frequency, the average dielectric constants of APA, APB, and APC films were 53.6, 35.4, and 28.9, respectively. Both the dielectric constant and dissipation factor decreased when frequencies increased. Generally, the dielectric constant decreases as the frequency increases, since it becomes difficult for the dipole to shift at high frequencies. [36] In addition, the dielectric constants of the thick films were rather low when compared with bulk (1250, measured by Advanced Ceramics Limited). The second phases

(Pb_2CrO_5 and TiO_2) might also cause this phenomenon because their dielectric constants were low, such as the dielectric constant of TiO_2 approximately 110 at 20°C.[38] In addition, Lipeles et al. [30] reported the Pb_2CrO_5 found as a phase in films and it could decrease the dielectric constants.

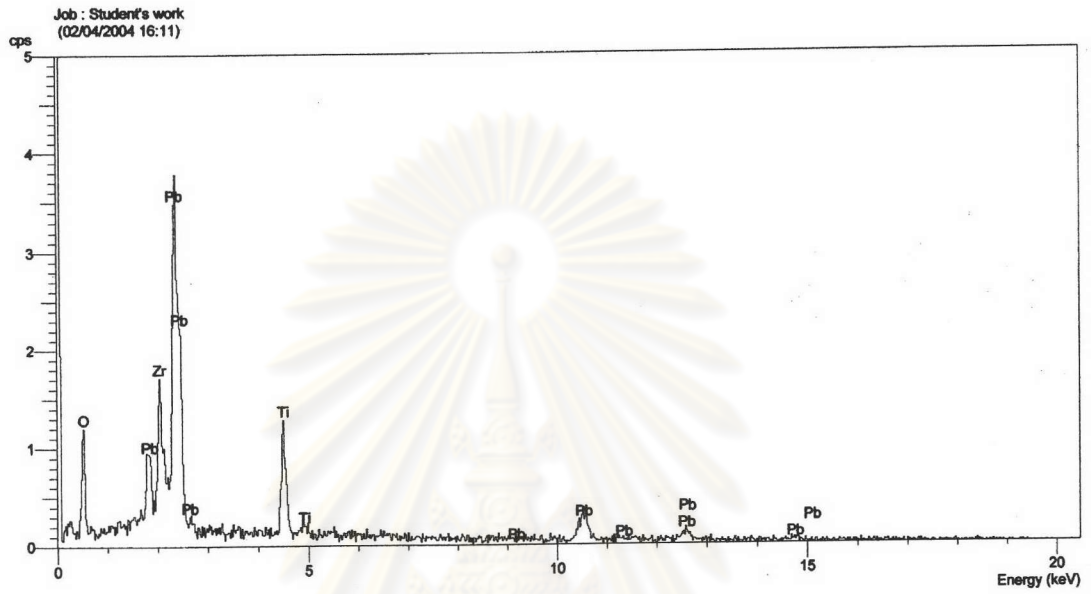

(a)

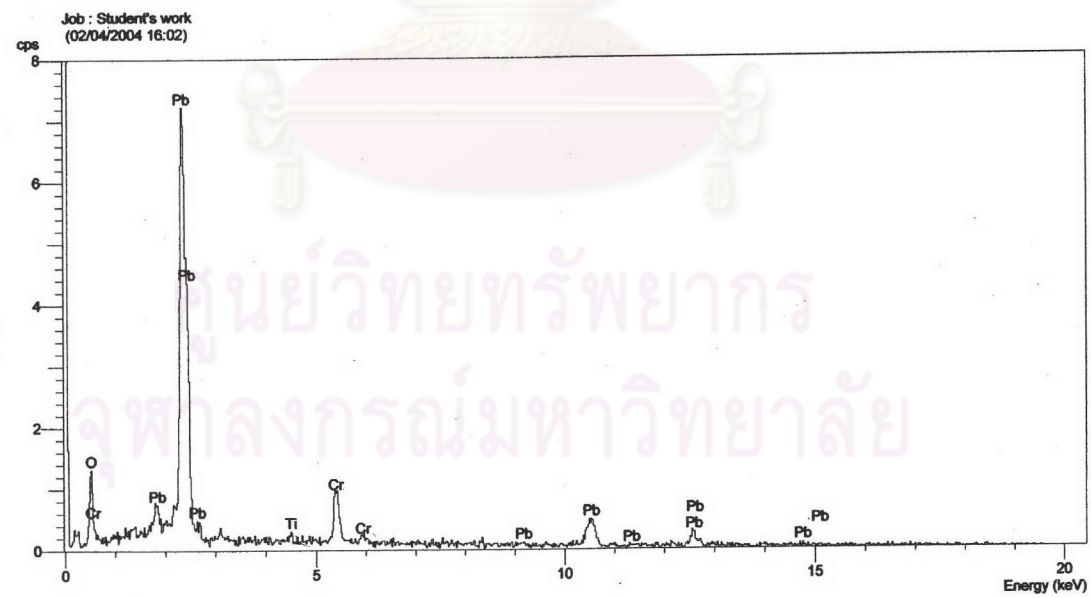

(b)

Fig. 4.8 EDS spectroscopy of APB thick film: (a) matrix grains and (b) abnormally large grains (second phase)

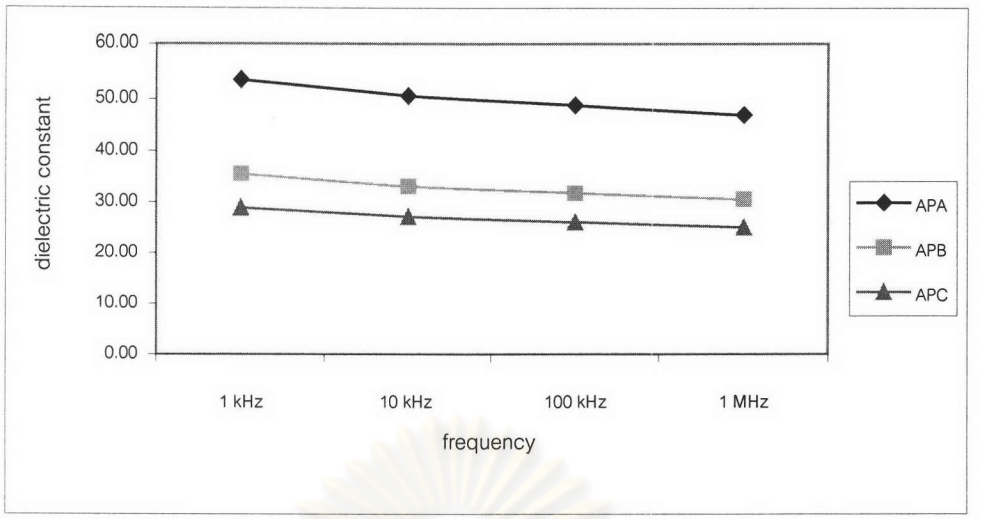

(a)

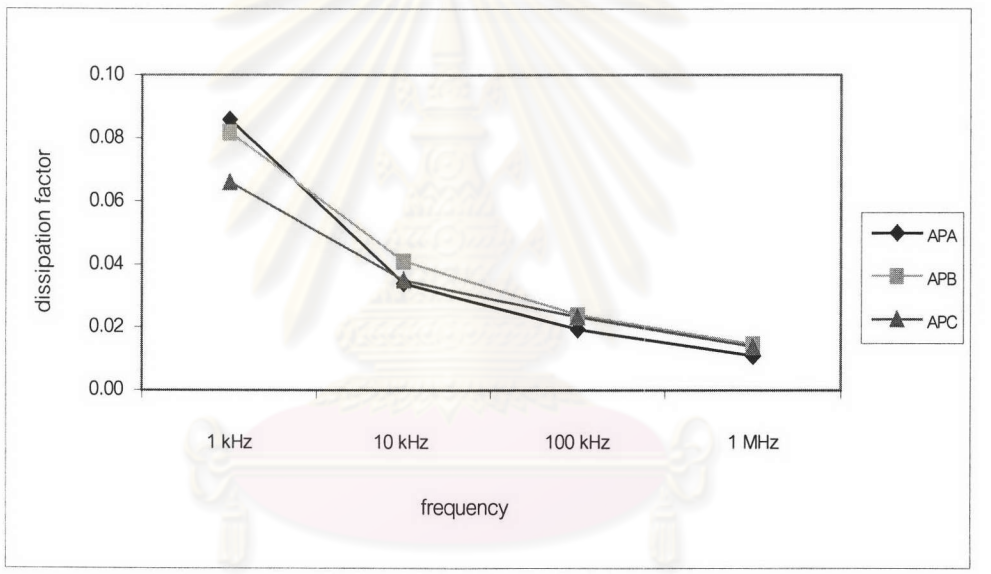

(b)

Fig. 4.9 Electrical properties of APA, APB, and APC thick films screen-printed onto stainless steel substrates after firing at 750°C for 1 hour; (a) dielectric constants and (b) dissipation factors.

4.3.2.2 ACL 4055 ferroelectric thick films

The phases and crystal structures of UPA, UPB, and UPC thick films were determined by the x-ray diffractometer. The x-ray diffraction patterns are shown in Fig. 4.10. All patterns have no significant discrepancy as they show a mixture of $Mg_{0.26}Pb_{0.95}Zr_{0.03}Nb_{0.60}O_{2.78}$ and $Pb_{2.5}Nb_2O_{7.5}$ similar to ACL 4055 powder. The impurity phases did not appear in the XRD study.

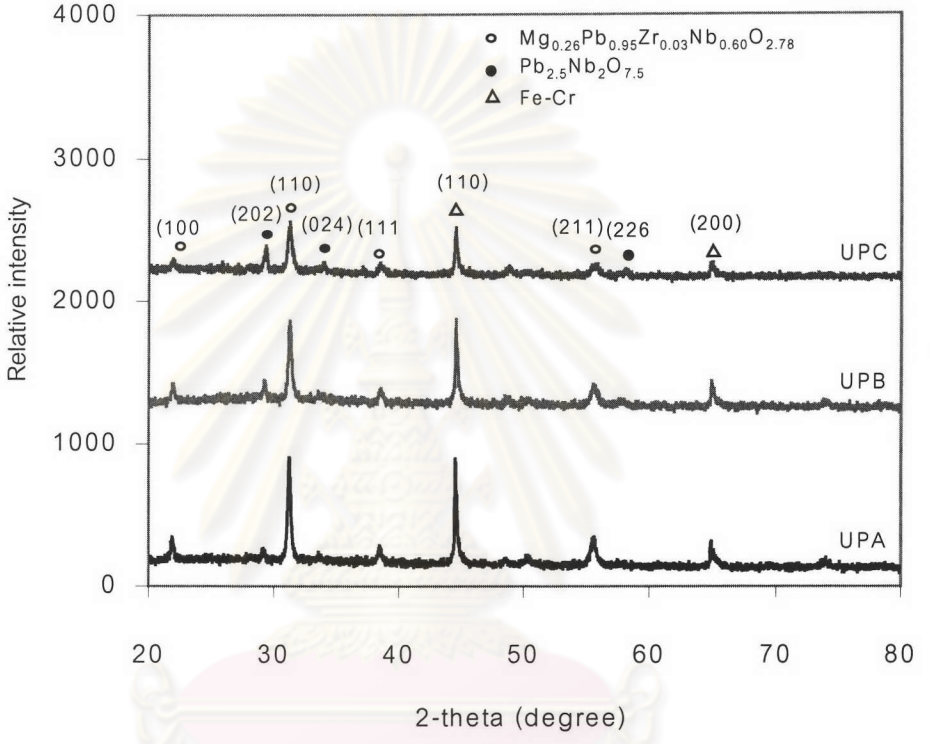

Fig. 4.10 XRD patterns of UPA, UPB, UPC thick films screen-printed onto stainless steel substrates after firing at 750°C for 1 hour.

SEM micrographs of all specimen surfaces are illustrated in Fig. 4.11. The grain sizes of UPA thick film seemed to be larger than UPB and UPC, respectively. In addition, abnormal grains (plate shape) were found in all thick films and they were remarkably seen in the UPC film. Therefore, the UPC paste was dried at 100°C and then fired at 750°C for 1 hour similar to the UPC thick film. After that, the fired UPC powder was ground in an alumina mortar and examined for the microstructure by SEM. The SEM micrographs of this powder are shown in Fig. 4.12 and no abnormal grains were present. From this result, the abnormal grains should be caused by the reaction between the stainless steel substrate and the thick film.

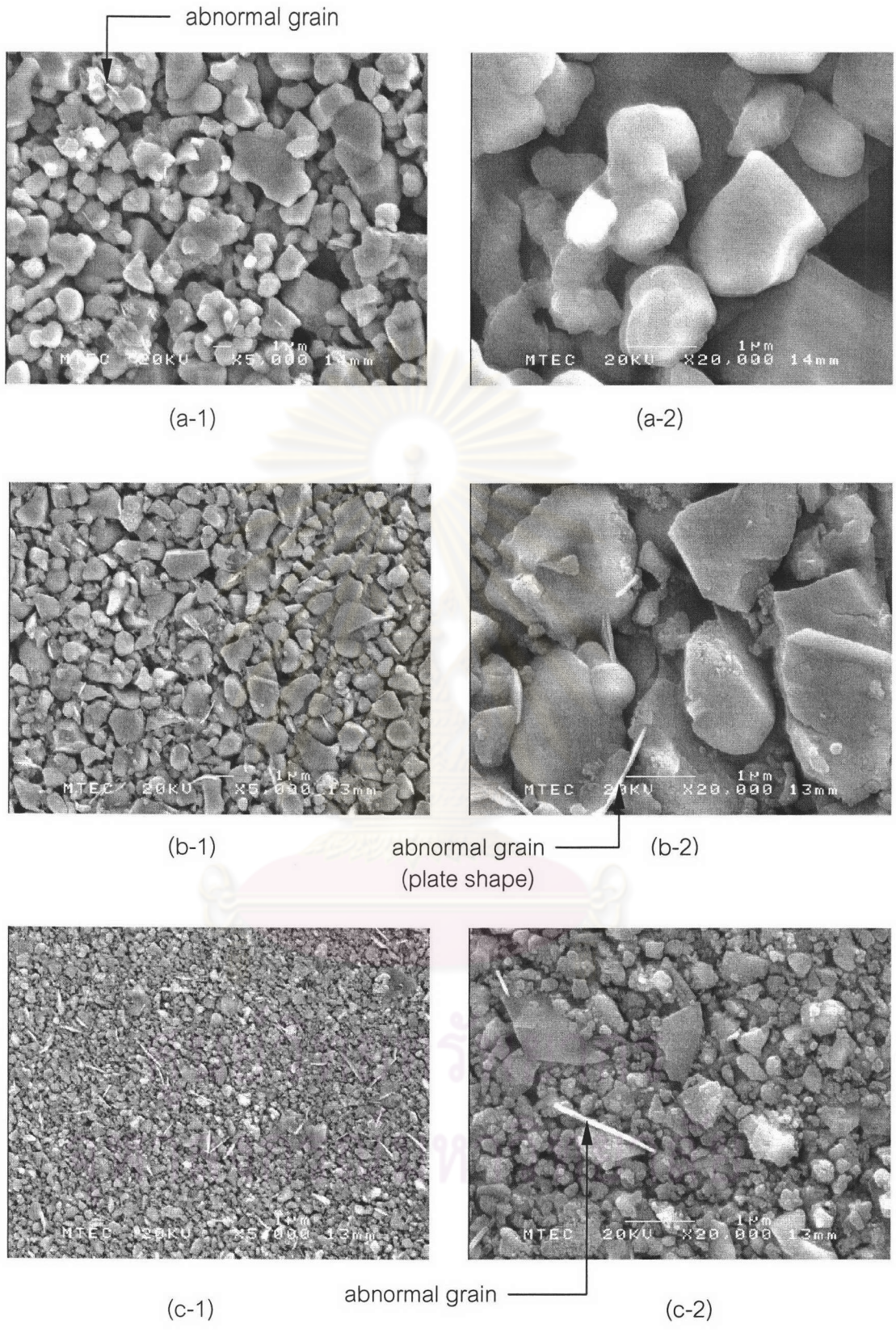

Fig. 4.11 SEM micrographs of (a-1,a-2) UPA, (b-1,b-2) UPB, and (c-1,c-2) UPC thick films screen-printed onto stainless steel substrates after firing at 750°C for 1 hour.

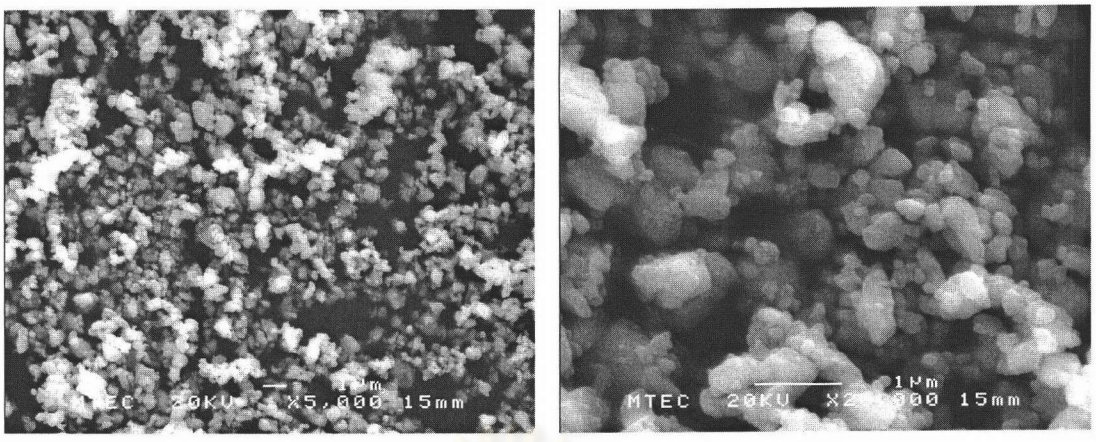

(a) (b)

Fig. 4.12 SEM micrographs of UPC paste after firing at 750°C for 1 hour: (a) X5,000 and (b) X20,000

From the EDS analysis, the abnormal grains (plate shape) were composed of Pb, Nb, Zr, Mg, Ti, Cr, and O as shown in Fig. 4.13. The Cr element should diffuse from the stainless steel substrate to the thick film and reacted with the other elements in the film. This reaction resulted in the abnormal grains (second phase).

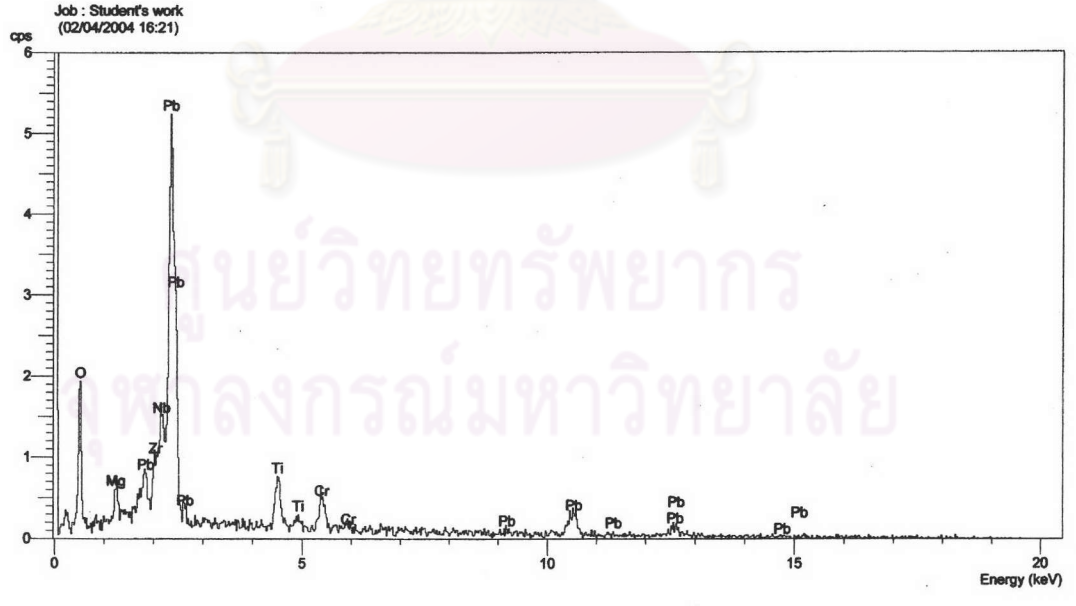

Fig. 4.13 EDS spectroscopy of the abnormal grain in the UPC thick film

Electrical properties of ACL 4055 thick film were measured by the impedance analyzer in similar manner as ACL 4040 thick films. The dielectric constants and dissipation factors are shown in Fig. 4.14. The dielectric constant of UPA thick film was the highest compared to others and also the dissipation factor of UPA was the lowest, especially at 1 kHz frequency. From observation, the UPA paste had high viscosity and was difficult to screen, so the solid loading was reduced from 85 to 84 percent by weight and so called UPA1. Its dielectric constants decreased when compared with UPA and UPB thick films. For example, the average dielectric constants of UPA, UPB, UPC, and UPA1 thick films were 81.5, 75.4, 51.7, 69.1, and the average dissipation factors were 0.07, 0.18, 0.21, and 0.15, respectively at 1 kHz frequency. In addition, the dielectric constants of ACL 4055 thick films (UPA, UPB, and UPC) were rather low when compared with bulk (5000, measured by Advance Ceramics Limited). These low values should cause by the abnormal grain and porosity.

From ACL 4040 and ACL 4055 thick film results, all films prepared from as-received powders; average particle sizes 4-5 μm gave the highest dielectric constant when compared with the films of 18 hour milled powders; average particle sizes 1-1.5 μm and the films of 72 hour milled powders; average particle sizes 0.3-0.4 μm at the same solid loading. These results corresponded to those of the SEM and XRD, which the films prepared from as-received powders had less quantities of abnormal grains. The abnormal grains (angular or plate shape) were high in ferroelectric thick films, which prepared from small particles (high specific surface area) of ferroelectric powders. This result might occur from the small particles were easily reacted with Cr of stainless steel substrates during sintering and resulted in the second phase (abnormal grain), which was one effect on dielectric property of ferroelectric ceramics.[33]

In addition, the films prepared from as-received powders contained rather large grains when compared with films prepared from 18 and 72 hour milled powders, when observed by SEM. From previous study, the K values increased with grain size but this was found in lead magnesium niobate (PMN)and lead iron niobate (PFN).[14,31] Apart from the grain size, the dielectric constants also depended on the reactivity of the ceramic powders. The highly reactive powders with high specific surface areas (small particle sizes) had large concentration of defects like dislocation, etc. Grain boundaries

and dislocations acted as anchors and immobilized the polar domains, thus decreasing the dielectric constants.[31]

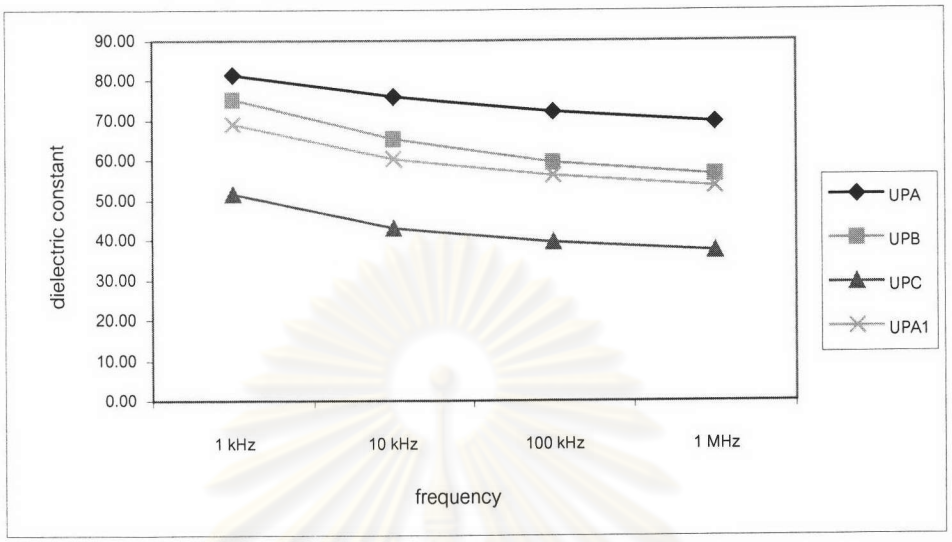

(a)

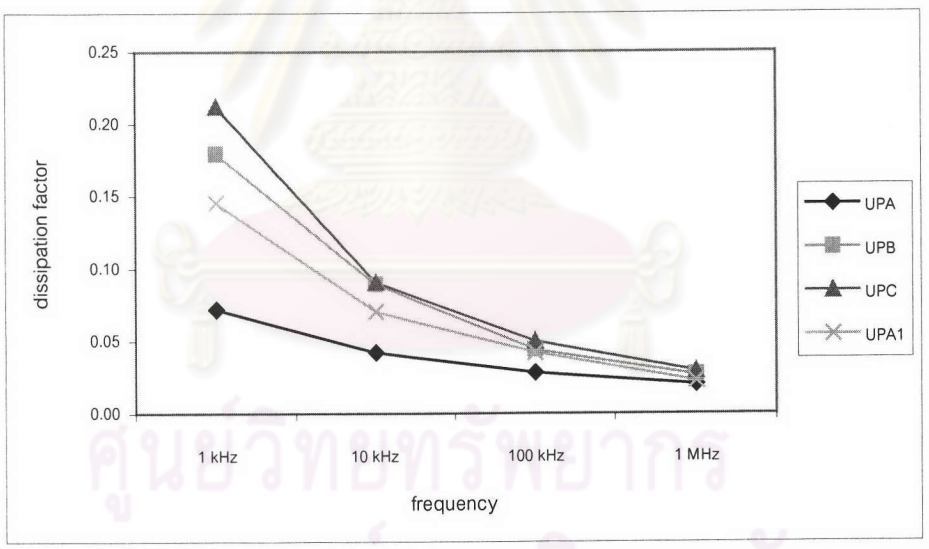

(b)

Fig. 4.14 Electrical properties of UPA, UPA1, UPB, and UPC thick films screen-printed onto stainless steel substrates after firing at 750°C for 1 hour; (a) dielectric constants and (b) dissipation factors.

4.3.3 Effect of ethyl cellulose on paste compositions

The 18 hour milled ACL 4055 powder was selected for this study. Although the thick film prepared from as-received ACL 4055 powder (UPA) showed the highest dielectric constant, the paste had high viscosity and its screenability was not good. It was also found that if the solid loading was decreased, the screenability was good. However, the dielectric constant of it (UPA1) was lower than UPB; prepared from 18 hour milled powder. For these reasons, the 18 hour milled powders were used throughout this experiment.

In this study, the amount of ethyl cellulose binder was varied in organic vehicles as shown in Table 4.4. The mixture of ACL 4055 powder and organic vehicle was stirred by stirring machine for 40 minutes. The ferroelectric pastes were screen-printed onto stainless steel substrates. The high viscosity pastes showed similar defect, i.e. small holes same as previous mentioned (Fig. 4.4) when they were screen-printed onto stainless steel substrates after 4 specimens in a row under same mask screen (5 x 5 mm^2). The optimum quantity of organic vehicle is shown in Table 4.5.

All the paste formulas in Table 4.5 could be screen-printed onto stainless steel substrates more than 15 pieces (5 x 5 mm^2) in a row under same mask screen. The viscosity of UPB9 paste formula; prepared with 11.04 wt%TE5 before printing looked fine but the paste on the top mask screen dried very fast, only after printing on 2 stainless steel substrates. The mask screen could not be used after that.

Table 4.4 Organic vehicle compositions

Organic vehicle formulas	Compositions	
	Terpineol (wt%)	Ethyl cellulose (wt%)
TE2	90.00 ± 0.01	10.01 ± 0.01
TE3	92.97 ± 0.02	7.04 ± 0.02
TE4	**94.96 ± 0.01**	**5.04 ± 0.01**
TE5	96.97 ± 0.02	3.04 ± 0.02

Table 4.5 Optimum organic vehicles in paste compositions

Paste formulas	Optimum organic vehicle
UPB	15.03 ± 0.01 wt% TE2
UPB7	13.05 ± 0.02 wt% TE3
UPB8	**12.03 ± 0.03 wt% TE4**

From Table 4.5, UPB8 formula was the best paste formula and it contained a small amount of organic vehicle while obtaining good surface appearance of thick films. The ethyl cellulose content in this formula was less than UPB and UPB7 and resulted in the highest solid loading. The small amount of binder is good for the microstructures of the films after firing to avoid too high porosity. If too much binder was added, undissolved binder would remain in the body and it could result in large pores after firing. [20] Furthermore, the organic binders strongly affected the rheology of the pastes as they could increase their viscosities.[20]

4.3.4 Effect of phosphate ester and frit on ferroelectric thick films

Phosphate ester was used as a dispersant, while frit ($PbO.B_2O_3.Bi_2O_3$) was used as a sintering aid. The paste formulas with phosphate ester and frit were called UPB8E and UPB8F, respectively. The compositions of these formulas were already shown in Table 4.2.

XRD patterns of UPB8E, and UPB8F are illustrated in Fig. 4.15. The patterns were similar to as-received ACL 4055 powders and there were no evidence of second phases. The present phases were identified as $Mg_{0.26}Pb_{0.95}Zr_{0.03}Nb_{0.60}O_{2.78}$ and $Pb_{2.5}Nb_2O_{7.5}$.

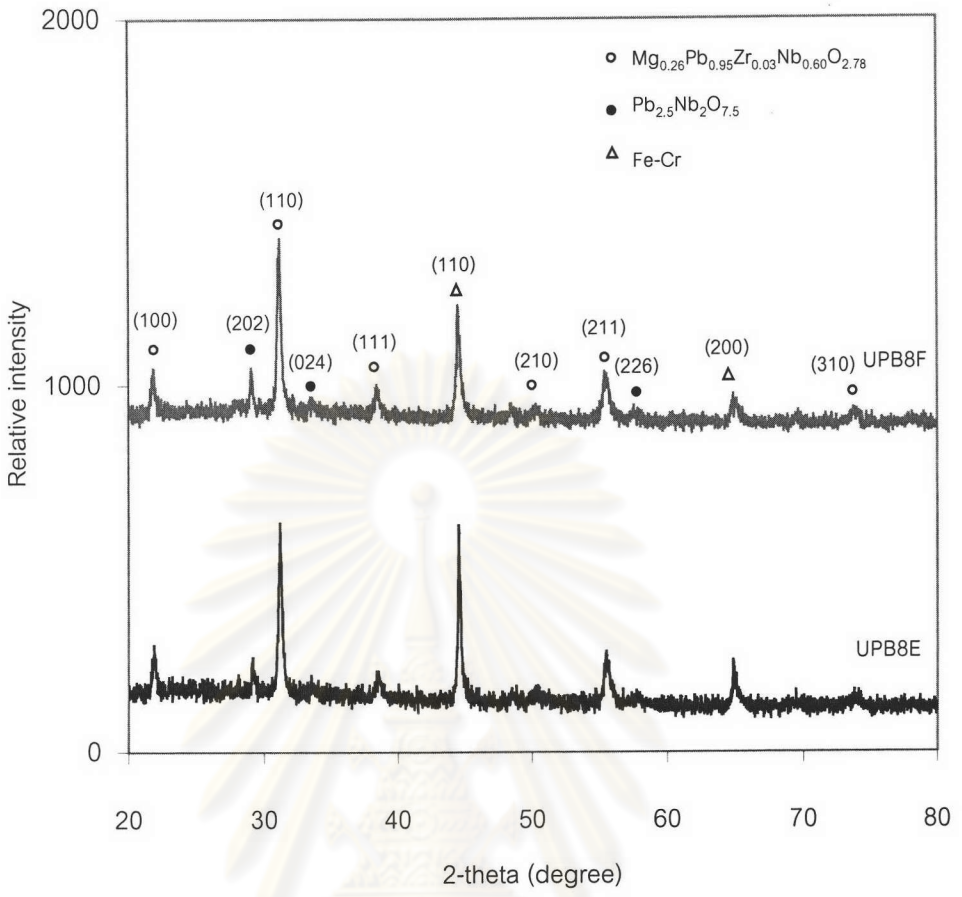

Fig. 4.15 XRD patterns of UPB8E and UPB8F thick films screen-printed onto stainless steel substrates after firing at 750°C for 1 hour.

SEM micrographs of the surface of UPB8E and UPB8F are shown in Fig. 4.16 and 4.17. The surface of UPB8E film was a more homogeneous than UPB8 (no phosphate ester and frit) and it was corresponded to surface roughness measurement, which measured by Dektak^{3}ST instrument. This measurement showed the surface roughness of UPB8 was 397 ± 123 nm and UPB8E was 208 ± 38 nm, which indicated that the phosphate ester improved the microstructural homogeneity of screen-printed thick film layers.[28] The magnification of SEM was increased from X500 to X20000 and the SEM micrographs of UPB8, UPB8E, and UPB8F are shown in Fig. 4.17. The necking and bonding between grains in UPB8F were slightly higher than UPB8 and they were corresponded to density measurement. This measurement showed the density of UPB8 was about 4.5 g/cm^3 and UPB8F was about 5.4 g/cm^3. These results concluded that the

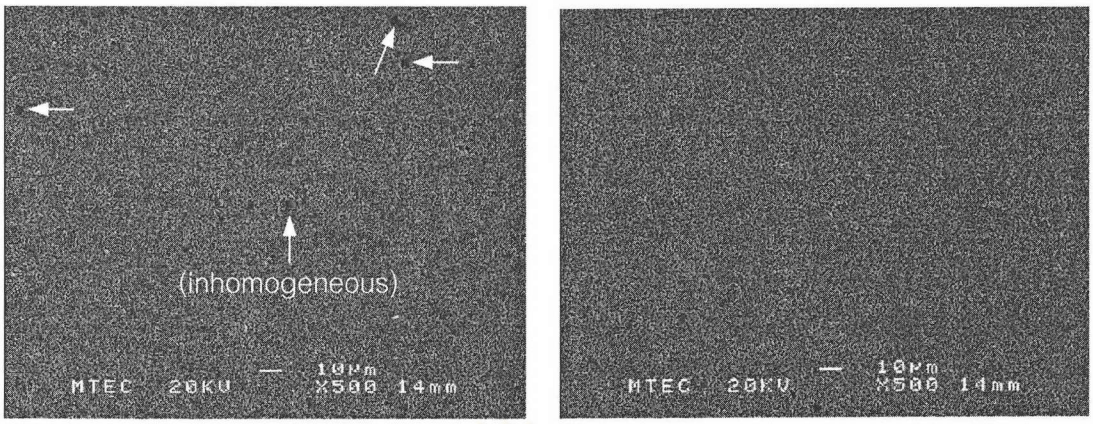

(a) (b)

Fig. 4.16 SEM micrographs of the surface of (a) UPB8 and (b) UPB8E thick films screen-printed onto stainless steel substrates after firing at 750°C for 1 hour.

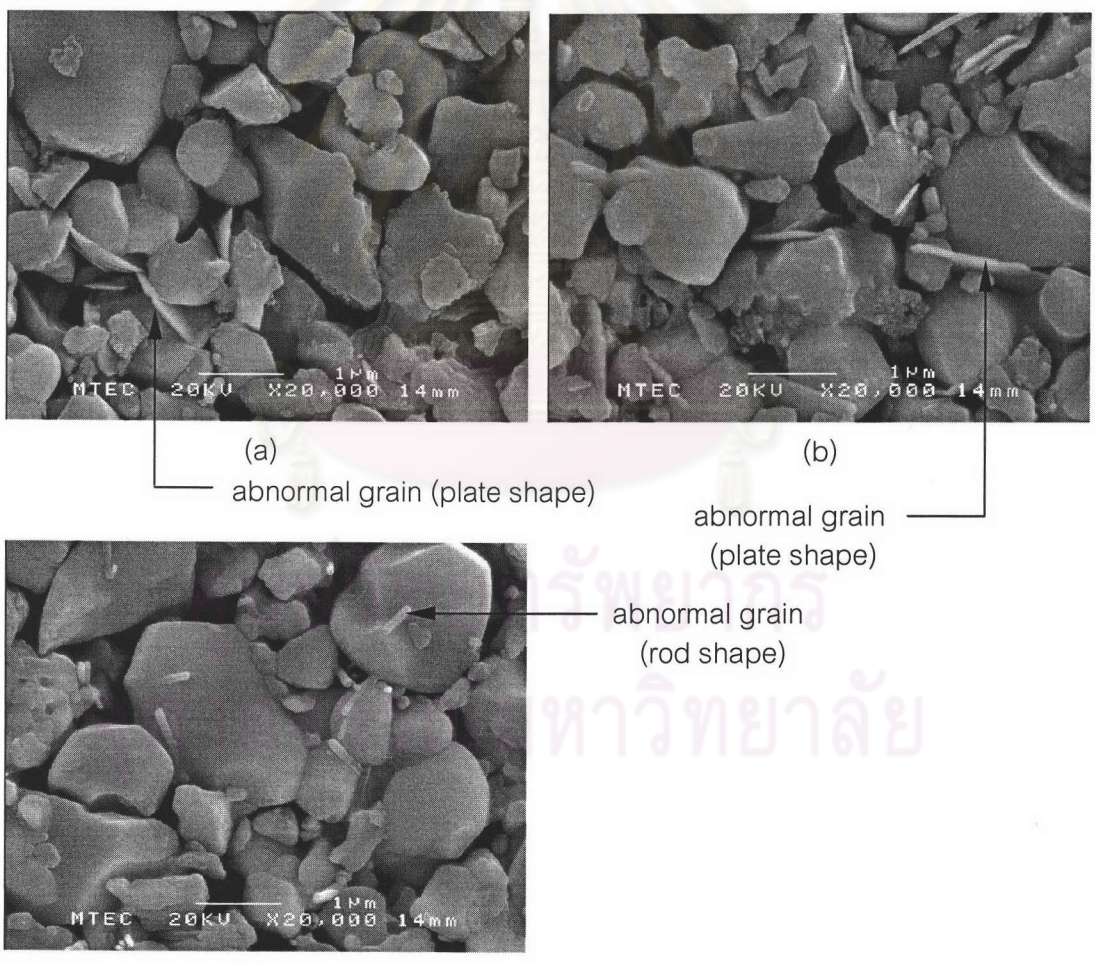

Fig. 4.17 SEM micrographs of the surface of (a) UPB8, (b) UPB8E, and (c) UPB8F thick films screen- printed onto stainless steel substrates after firing at 750°C for 1 hour.

frit could increase the densification of the thick film. However, the abnormal grains (plate shape and rod shape) were found in UPB8, UPB8E, and UPB8F respectively.

The electrical properties of them are shown in Fig.4.18. The gold was coated on UPB8 ferroelectric thick films for 120 sec in the first stage. However, they had a problem associated with electrode continuity, the films peeled off during electrical measurement. Therefore the sputtering time was increased from 120 sec to 150 sec for UPB8, UPB8E, and UPB8F thick films in order to solve this problem. The sputtering time of 150 sec was used throughout this experiment. The dielectric constants of UPB8E and UPB8F thick films were higher than UPB8 at all frequencies. Also, the dissipation factors of them were rather high. For example, the average dielectric constants of UPB8 (120 sec), UPB8 (150 sec), UPB8E (150 sec), and UPB8F (150 sec) thick films at 1 kHz frequency were 98.4, 150.5, 318.3, 248.0, while the average dissipation factors were 0.27, 0.27, 0.22, and 0.19, respectively.

In this study, the dielectric constant of the films, which were added with phosphate ester increased. This is because the very small addition of the phosphate ester to the paste formulation dramatically decreases viscosity, allowing the formulation of better printability paste with higher solid concentration and homogeneous film surface.[28] For UPB8F formula, the dielectric constant of this formula was higher than UPB8 too. They indicated that the frit ($PbO.B_2O_3.Bi_2O_3$) could improve the densification of the films as shown in Fig. 4.17. It should induce liquid phase below the sintering temperature and promoting densification and coarsening at low temperature.[32] The increasing densification (decreasing porosity) enhances the dielectric constant.[23] In addition, the low sintering temperature is good in the sense that the reaction between the substrates and the films and PbO evaporation are suppressed.

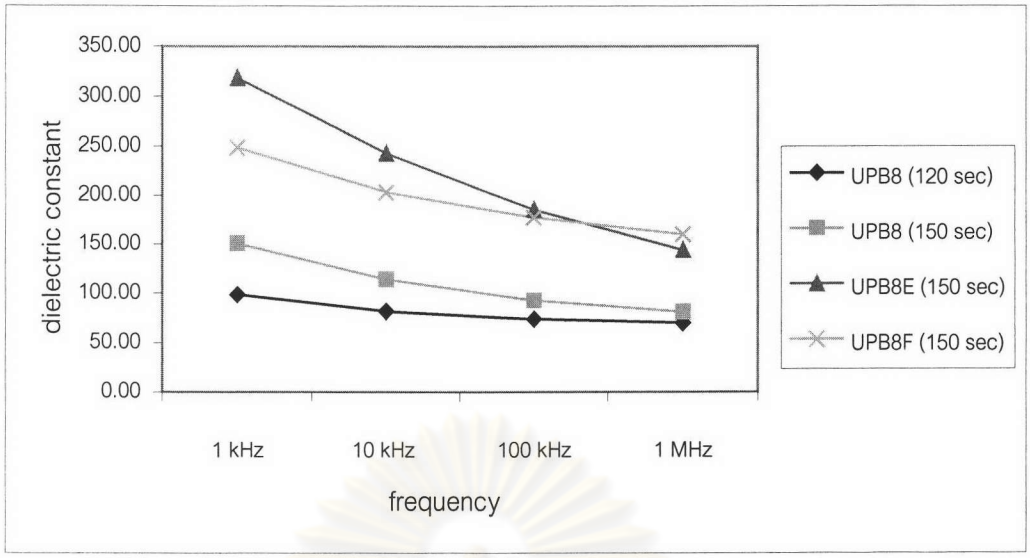

(a)

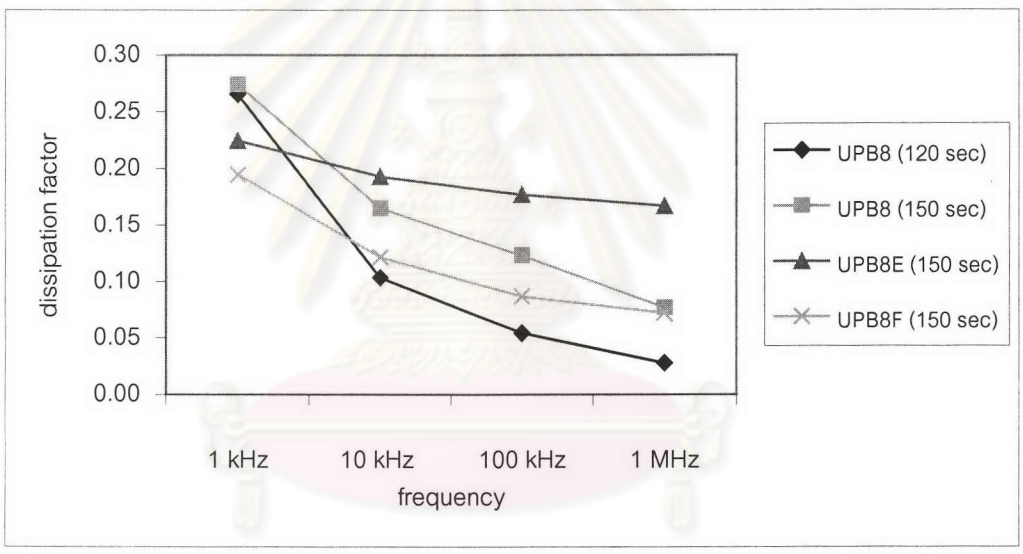

(b)

Fig. 4.18 Electrical properties of UPB8, UPB8E, and UPB8F thick films screen-printed onto stainless steel substrates after firing at 750°C for 1 hour; (a) dielectric constants and (b) dissipation factors.

4.3.5 Effect of sintering temperature on ferroelectric thick films

The phosphate ester and frit were found useful for the thick films in the preliminary test. In this study, they were mixed together with Pb-based ferroelectric powders and organic vehicles, and a paste was called UPB8EF1 formula. The ferroelectric paste was screen- printed onto stainless steel substrates approximately 25 pieces (5 x 5 mm^2) with the same mask screen. Ferroelectric thick films on the substrates were fired at 680°C, 750°C, 800°C, and 850°C for 1 hour.

The thick films were characterized for phases and crystal structures, and XRD patterns are shown in Fig. 4.19. They showed a mixture of $Mg_{0.26}Pb_{0.95}Zr_{0.03}Nb_{0.60}O_{2.78}$ and $Pb_{2.5}Nb_2O_{7.5}$ phases. The Fe_2O_3 phase was also found when the thick films were fired at 850°C, due to the reaction of iron and oxygen from air at high temperature.

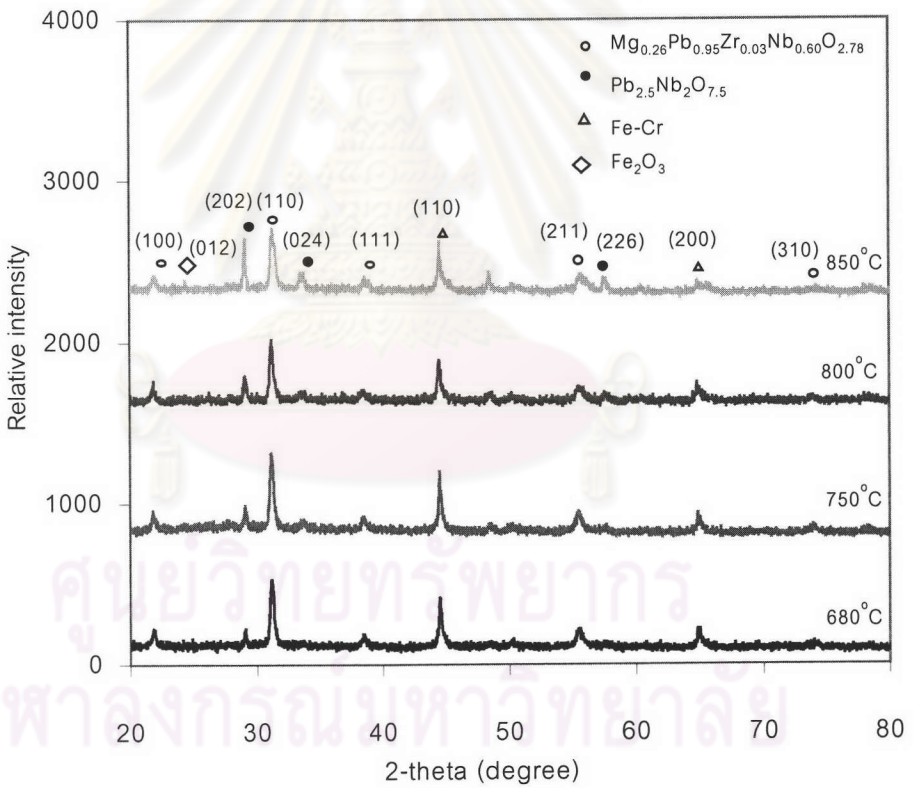

Fig. 4.19 XRD patterns of UPB8EF1 thick films screen-printed onto stainless steel substrates after firing at 680°C, 750°C, 800°C, and 850°C for 1 hour.

SEM micrographs of them are shown in Fig.4.20. High porosity was found when the thick films were fired at 800°C and 850°C. The abnormal grains occurred in the thick films similar to UPB8F, but they were only found in these films after firing at 750°C and 800°C. They were remarkably appeared when the thick films were fired at 800°C. However, they were not found in the films fired at 680°C and 850°C. In addition, the thick films cracked when they were fired at 850°C for 1 hour as shown in Fig. 4.21.

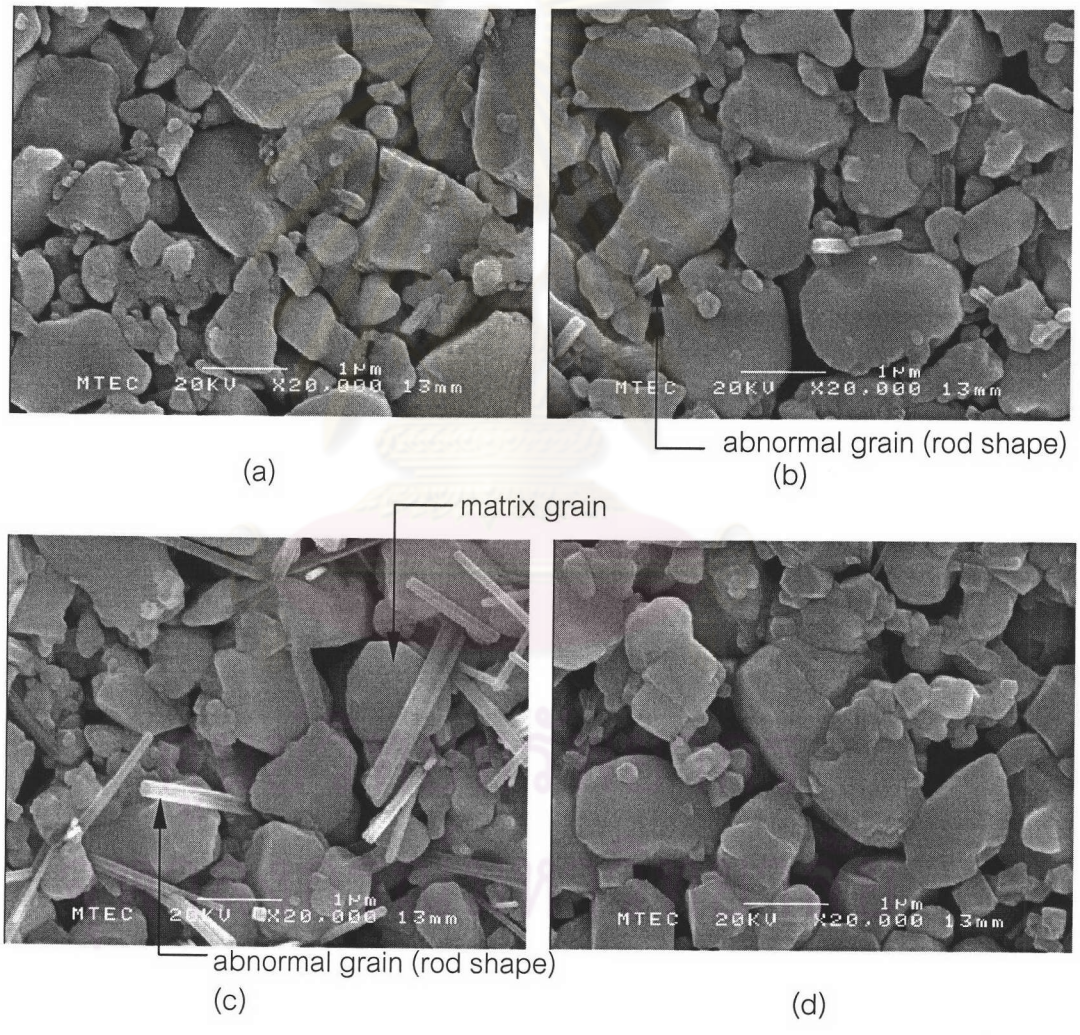

Fig. 4.20 SEM micrographs of the surface of UPB8EF1 thick films screen-printed onto stainless steel substrates after firing at (a) 680°C, (b) 750°C, (c) 800°C, and (d) 850°C for 1 hour.

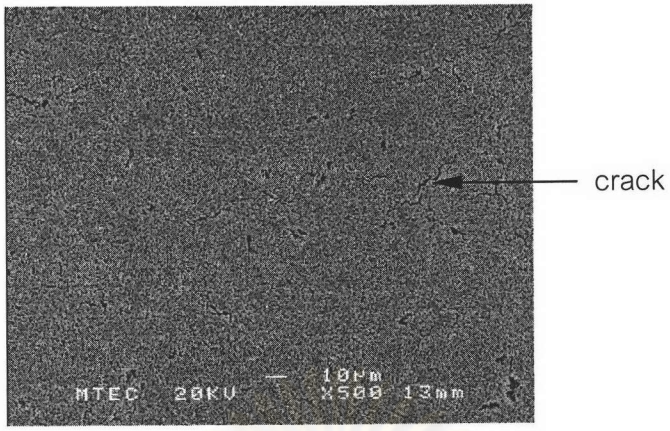

Fig. 4.21 SEM micrographs of the surface of UPB8EF1 thick films screen-printed onto stainless steel substrates after firing at 850°C for 1 hour.

In order to investigate how the abnormal grain; rod shape was formed, the UPB8EF1 paste was dried at 100°C and fired at 750 and 800°C for 1 hour. The UPB8EF1 powder was ground in an alumina mortar and then characterized by SEM. The SEM micrographs are shown in Fig. 4.22 and no the abnormal grains were found in the paste. From this result, it could be conclude that the abnormal grain in Fig. 4.20 might come from the chemical reaction between the thick films and the stainless steel substrates.

The abnormal grains (rod shape) were characterized by EDS technique. From EDS result as shown in Fig. 4.23, it was evident that the abnormal grains could possibly be a second phase of Mg-Cr-O compounds as the Mg, Cr, and O peaks were clearly found in the patterns when compared with matrix grains.

The electrical properties were characterized at room temperature and are shown in Fig. 4.24. Dielectric constants and dissipation factors of the thick films decreased when frequencies increased. The average dielectric constants of 680°C, 750°C, 800°C, and 850°C fired films were 228.6, 351.6, 272.4, and 116.4 at 1 kHz frequency and the average dissipation factors at 1 kHz frequency were 0.12, 0.15, 0.17, and 0.41. It was noticed that there was no difference in the values of dissipation factors of the films fired at 680-800°C, except that at 850°C.

The sintering temperature of 850°C was not suitable for the thick films because of the crack. The cracked films might cause the low dielectric constants and high

dissipation factors. The sintering temperature of 750°C was the most suitable for UPB8EF1 thick films because the films showed the highest dielectric constant (351.56). This dielectric constant (351.6) of UPB8EF1 thick films, which were fired at 750°C for 1 hour was rather high when compared with previous study. Wangchokphadung et al.[13] reported the dielectric constant of PZT thick film on the stainless steel substrate was 110 and the dissipation factor was 0.25.

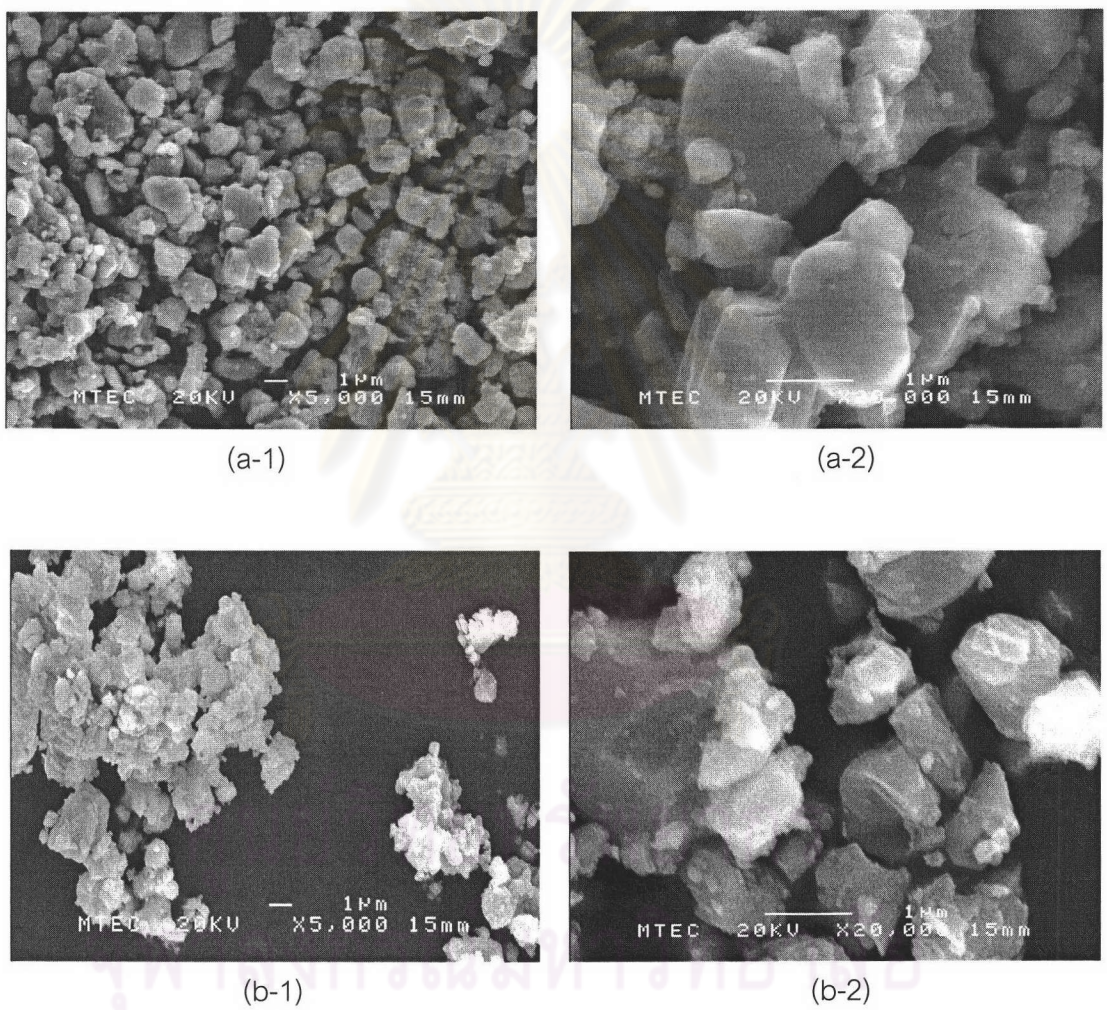

Fig. 4.22 SEM micrographs of UPB8EF1 paste after firing at 750°C and 800°C for 1 hour; (a-1) 750°C,x5,000, (a-2) 750°C, x20,000, (b-1) 800°C, x5,000, and (b-2) 800°C, x20,000

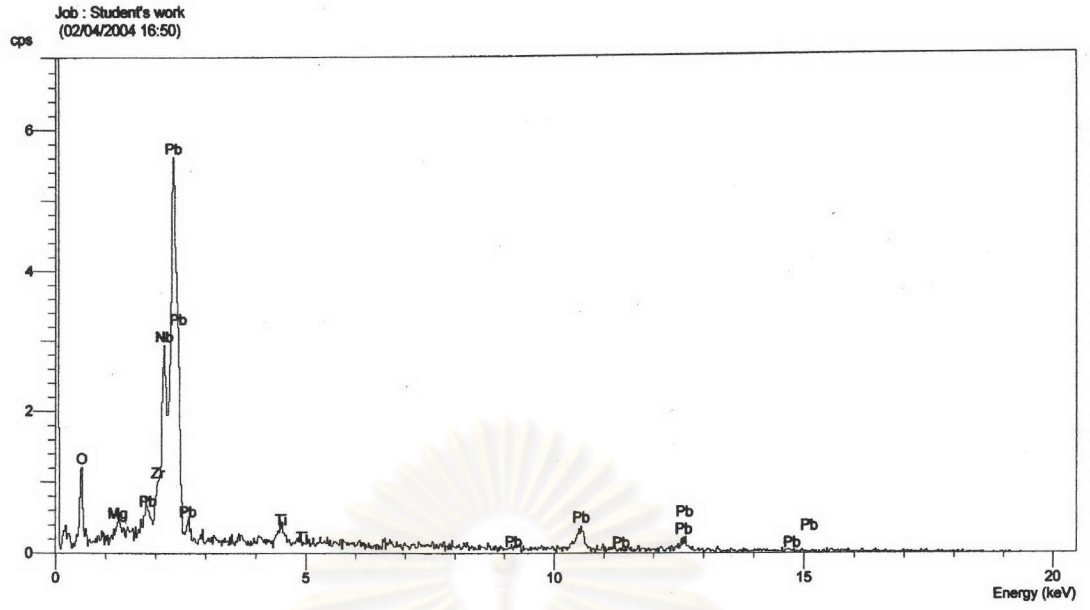

(a)

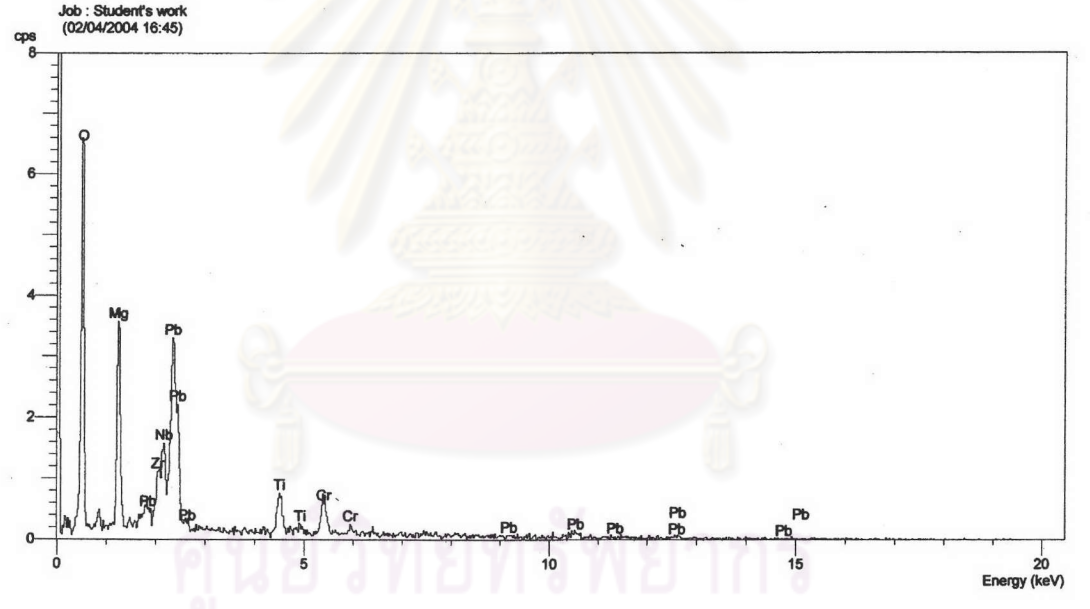

(b)

Fig. 4.23 EDS spectroscopy of UPB8EF1 thick film after firing at 800°C for 1 hour: (a) matrix grain and (b) abnormal grain (rod shape)

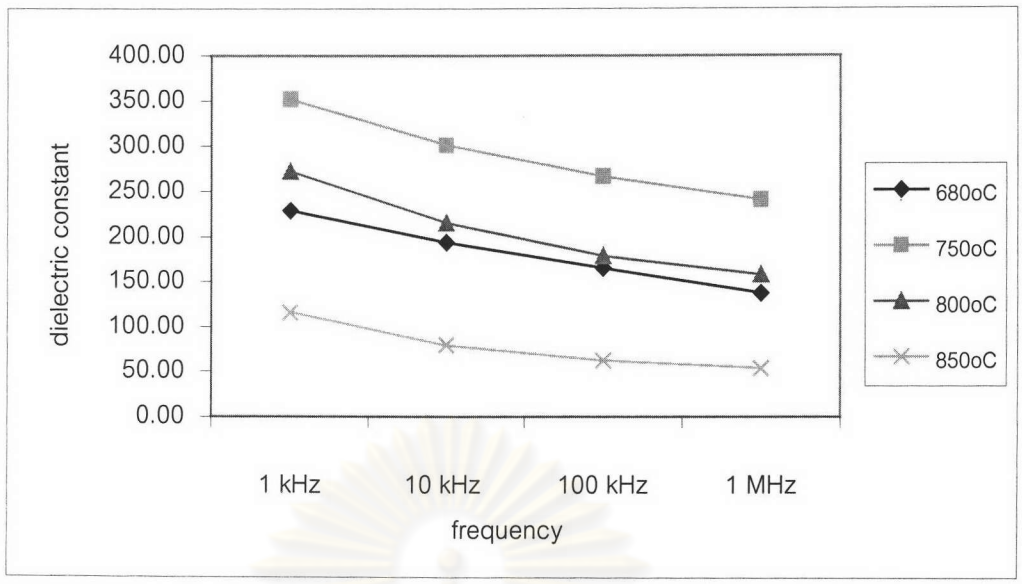

(a)

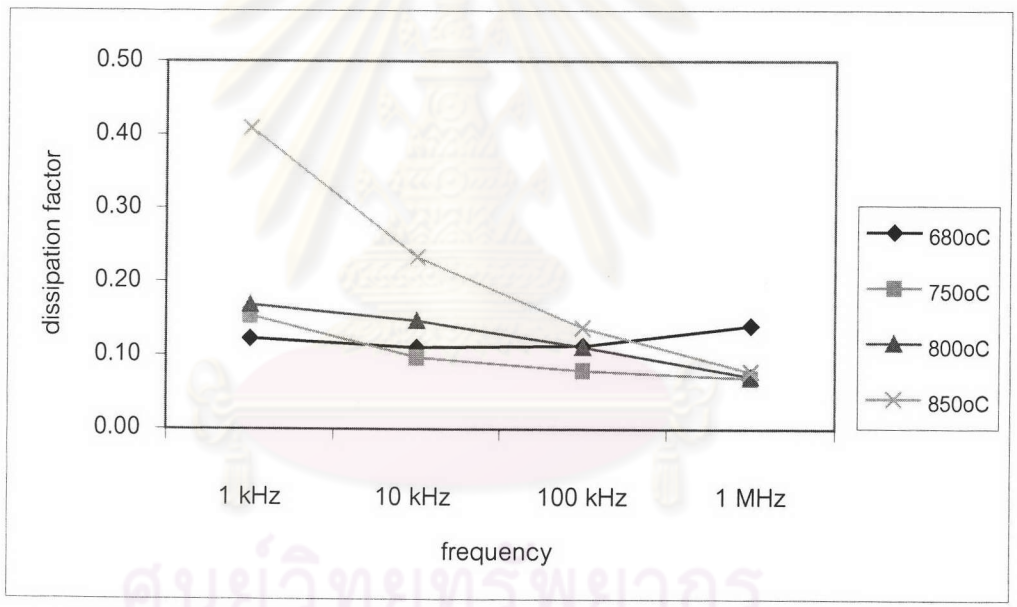

(b)

Fig. 4.24 Electrical properties of UPB8EF1 thick films screen-printed onto stainless steel substrates after firing at 680°C, 750°C, 800°C, and 850°C for 1 hour; (a) dielectric constants and (b) dissipation factors.

However, the ferroelectric thick films should give much a higher dielectric constant than this value (351.6). We assumed the oxide layer may occur between the thick film and the stainless steel substrate since ceramic-metal systems where the metal was able to react with the ceramic and the reaction conditions (temperature, time and ambient) determine whether or not new phases will be formed.[33] If this oxide occurred under the thick film then a series capacitor C was formed with effective permittivity lower than expected. Therefore, it caused a decrease in the dielectric constant.

To prove this assumption, the UPBEF1 thick film was cut by diamond saw. The cross-sectioned was examined by SEM and determined elements by EDS technique. The cross-sectioned is shown in Fig. 4.25 and the patterns of EDS as shown in Fig. 4.26.

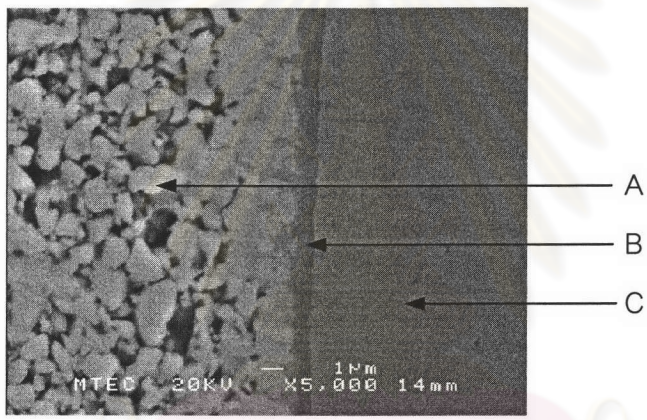

Fig. 4.25 SEM micrographs of the cross-sectioned of UPB8EF1 thick film screen-printed onto stainless steel substrates after firing at 750°C for 1 hour.

In Fig. 4.25, A, B, C regions were the UPB8EF1 thick film, the interfacial layer of some kind, and the stainless steel substrate, respectively. From EDS, B region showed strong peaks of O, Pb, Cr, Fe elements as shown in Fig. 4.26. The interfacial layer (B region) of a thickness of 1.0 μm should be an oxide layer from reaction between these elements that was corresponding the previous hypothesis. Therefore, the oxide layer was one of main reason to give rise to low dielectric constant.

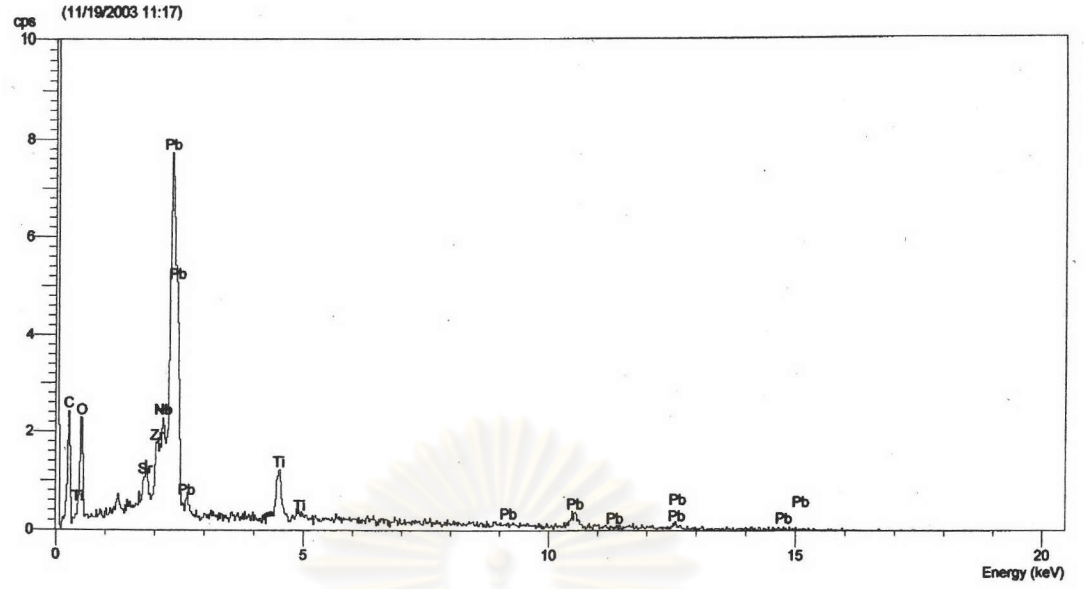

(a)

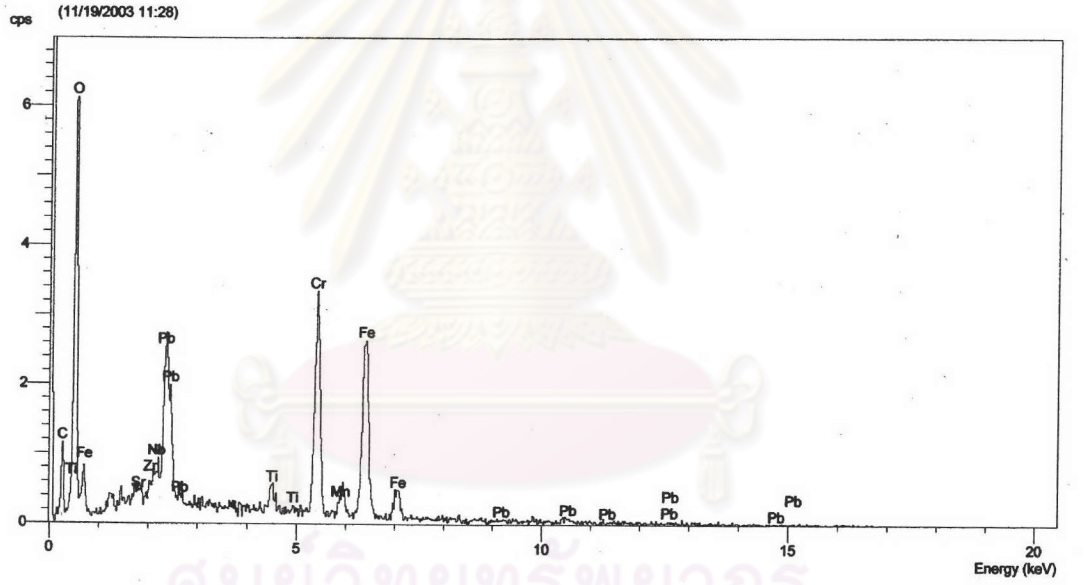

(b)

Fig. 4.26 EDS spectroscopy of the cross-sectioned of UPB8EF1 after firing at 750°C for 1 h (Fig. 4.25): (a) UPB8EF1 thick film and (b) interfacial layer (oxide layer)

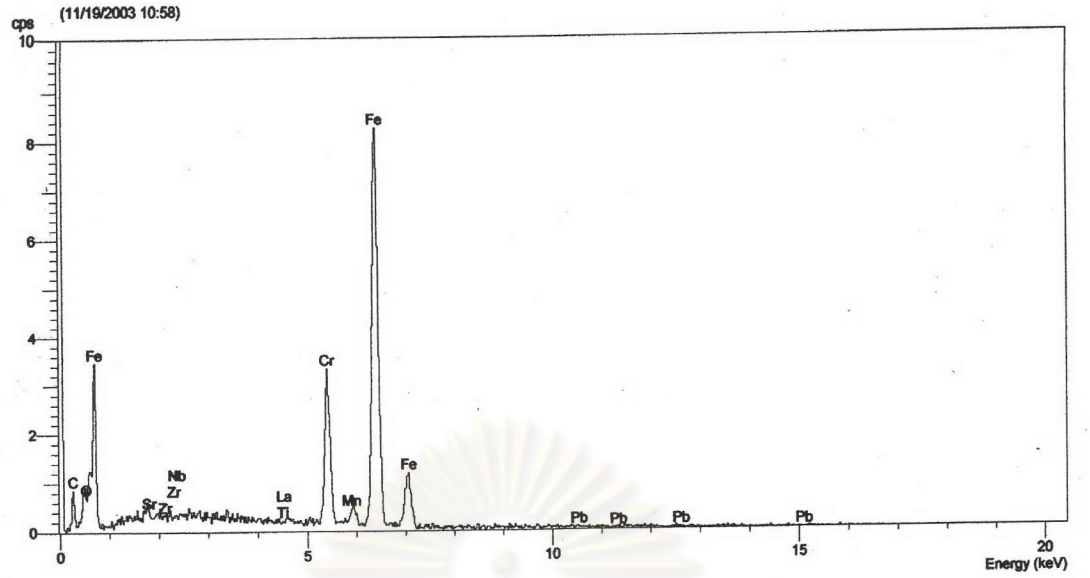

(c)

Fig. 4.26 EDS spectroscopy of the cross-sectioned of UPB8EF1 after firing at 750°C for 1 h (Fig. 4.25): (c) stainless steel substrate